

# Elastic Continuum Solution of Stacked Pile Model for Axial Load-Displacement Analysis

Fawad S. Niazi<sup>1</sup> and Paul W. Mayne<sup>2</sup>

School of Civil and Environmental Engrg., Georgia Institute of Technology, Atlanta, Georgia, USA

<sup>1</sup>E-mail: fniazi6@gatech.edu

<sup>2</sup>E-mail: paul.mayne@gatech.edu

**ABSTRACT:** In a companion paper, new sets of shear stiffness reduction curves developed from the back-analyses of 299 static axial pile load tests were presented towards the implementation of a non-linear load-displacement (Q-w) response analysis within the framework of Randolph-type closed-form elastic continuum solution. These curves were developed with the following underlying assumptions: (1) soil stiffness is linear with depth (although certain situations may portray a different trend), and (2) the back-analyzed field stiffnesses can be obtained keeping the operative modulus profile constant throughout the loading (even though shaft resistance is expected to be mobilized prior to the end bearing). In an effort to make some improvements with respect to these conditions, certain provisions of the elastic continuum solution are exploited to present a methodology for drawing the stiffness reduction curves as functions of depth. These curves are further utilized in modeling the pile as a stack of smaller shaft segments embedded in multi-layered soils, where each layer is assigned its own distinctive averaged stiffness. The load-displacement analysis of all pile segments, associated with their adjacent soil layers, can thus be performed using the stiffness reduction curves applicable to their respective depths. The overall load-displacement response is obtained through integration of the analysis result of all layers. Flow charts are presented detailing steps for plotting the depth-dependent stiffness reduction curves. Similarly illustrative figures are included showing the procedures for implementing the stacked pile model for compressible as well as rigid piles.

**KEYWORDS:** Pile foundations, Displacements, Shear modulus, Shear wave velocity, Soil stiffness, Layered soil profile

## 1. INTRODUCTION

In a companion paper [Niazi and Mayne (2015)], a new scheme of shear modulus reduction curves [i.e., normalized shear modulus ( $G/G_{max}$ ) vs. pseudo-strain ( $\gamma_p = w_t/d$ )] was presented for use in the non-linear axial load vs. displacement (Q-w) analysis of pile foundations within an elastic continuum solution. These schemes were derived via back-analysis from pile load test data. The  $G$  and  $G_{max}$  values in this framework represent the operative and initial shear moduli, respectively, along the pile shaft at the reference elevation of full pile length (i.e., at depth  $z = L$ ), while  $w_t$  and  $d$  are the top displacement and pile diameter, respectively. As such, the following vital and rationally acceptable assumptions were made in the back-analysis approach:

- The back-analyzed field stiffness can be obtained keeping the modulus variation factor ( $\rho_E$ ) constant, where  $\rho_E = G_M/G_L$ ;  $G_M$  = shear modulus at mid-depth of the pile (at  $z = L/2$ ); and  $G_L$  = shear modulus at the full pile length (at  $z = L$ ). It implies that moduli all along the shaft and that around the base decreases at the same rate. In actual field situations, the shaft resistance is expected to mobilize prior to the end bearing, leading to faster reduction of  $G$  in the upper layers than those near the base, thus manifesting the concept of progressive failure with depth.
- The soil stiffness is linear with depth. This assumption was adopted from the shear wave velocity ( $V_s$ ) profiles of the sites in the database, which provided  $G_{max}$  readings. A predominant majority of the sites validated this assumption by presenting either linear or general Gibson types of soil profiles. However, it is expected that some special sites may portray different trends.

In the case of non-uniform or non-linear stiffness profiles of a multi-layered soil medium, it may be prudent to adopt a stacked pile model, where the pile is treated as separate segments of shorter piles stacked one above the other through different layers. In this case, the stiffness profiles of different layers of smaller thicknesses than the overall pile length may suitably be assumed uniform, and their separate Q-w analyses performed, followed by their integration into the overall Q-w evaluations. On the other hand, the effects of progressive failure can be subsumed in this stacked pile model by making slight modifications to the modulus reduction schemes

presented in Niazi and Mayne (2015). Such modifications are possible by adopting certain provisions of the original elastic continuum model by Randolph and Wroth (1978; 1979), and Randolph (2007).

The aim of this paper is to present a stacked pile model for evaluating the axial pile Q-w as a function of depth within multi-layered soil media.

## 2. REVIEW OF ELASTIC CONTINUUM SOLUTION FOR PILE LOAD DISPLACEMENT RESPONSE

The basic formulation of analytical elastic continuum closed-form solution by Randolph and Wroth (1978; 1979), and Randolph (2007) was summarily presented in Niazi and Mayne (2015). This solution, reproduced in eq. (1), was developed for piles embedded in a linear elastic two-layered soil model with the boundary lying at the pile base (see Figure 1a, where explanation of various terms is also given).

$$w_t = \frac{Q_t \left[ 1 + \frac{4\eta \tanh(\mu L)}{\pi\lambda(1-\nu_s)\xi(\mu L)} \frac{r_o}{r_o} \right]}{G_L r_o \left[ \frac{4\eta}{(1-\nu_s)\xi} + \frac{2\pi\rho_E \tanh(\mu L)}{\zeta(\mu L)} \frac{r_o}{r_o} \right]} \quad (1)$$

The top displacement ( $w_t$ ) may be obtained for an applicable value of the applied top load ( $Q_t$ ) by utilizing a suitable shear modulus reduction scheme, such as the one presented in Niazi and Mayne (2015). Here, the displacement field of soil around the pile shaft has been modeled via shearing of infinite concentric cylinders of differentially increasing radii with maximum influence radius modeled as shown in Figure 1b. This follows from the important observations noted by Cooke (1974), Cooke et al. (1979), and Frank (1975) that the load transferred to the adjacent soil through shearing stresses mobilized along the pile shaft extends radially beyond the close proximity of the pile, and that there exists some magical radius ( $r_m$ ) around the pile at which these stresses become negligible. Randolph and Wroth (1978; 1979) noted that within this radial distance, the shear stresses and the resulting displacements decrease logarithmically with increasing distance from the pile shaft surface.

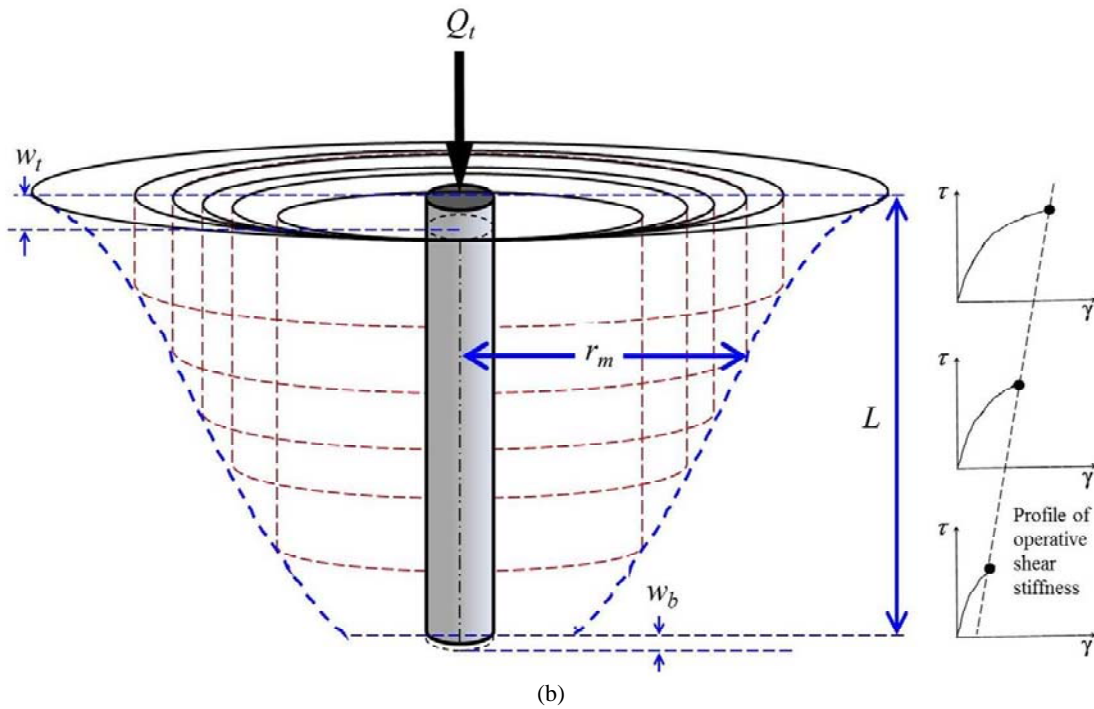
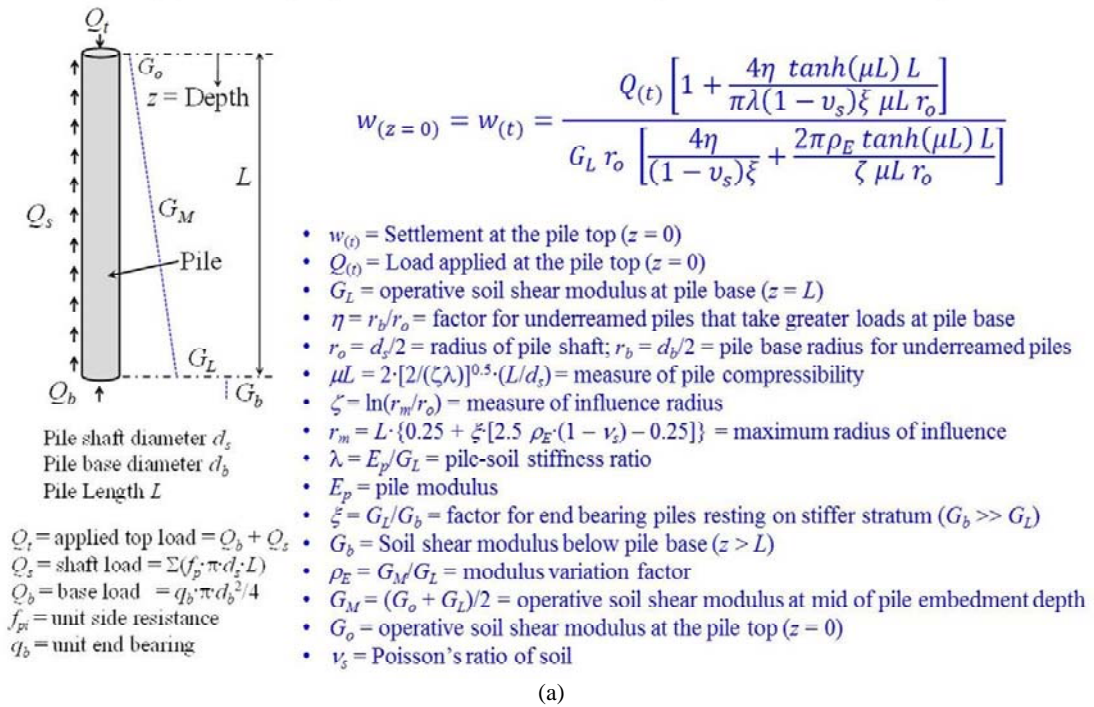


Figure 1 Elastic continuum model for axial pile displacements analysis in a linear elastic two layered soil model (after Randolph and Wroth 1978; 1979), Randolph (2007): (a) Randolph pile model of axial pile load-displacement relationship, and (b) displacement field model and profile of maximum influence radius.

As the load transferred to the pile shaft diminishes with depth, so do the shearing stresses, influence radii, axial displacements, and their corresponding reductions in the operative shear stiffness. The shape of the  $r_m$  profile, thus hypothesized, is attributable to the horizontal and vertical inhomogeneity of shearing stresses explained by the following: (1) fundamental conjecture that the soil stiffness generally increases with depth describing greater resistance to shearing deformations in deeper layers, and (2) the load applied from the pile top diminishes with depth leaving lesser loads to shear the stiffer soils adjacent to the pile shaft in deeper layers.

Also shown in Figure 1b is the profile of operative shear stiffness ( $G$ ) [on qualitative shear stress ( $\tau$ ) vs. shear strain ( $\gamma$ ) plots] as a function of depth along the pile shaft. Accordingly, the reduction of operative shear stiffness ( $G$ ) varies inversely with depth ( $z$ ) below the ground surface.

### 3 EXTENDED CONTINUUM SOLUTION TO STACKED PILE IN MULTI-LAYERED SOILS

#### 3.1 Shear Modulus Reduction Curves for Progressive Load Transfer as Function of Depth

Implicit and inherent in the elastic continuum solution are certain provisions whereby it may be employed for predicting the displacements as a function of depth (z) below the ground surface. Accordingly, as shown in eq. (2), the term L, which represents the total embedded length of the pile may be replaced with (L - z).

Furthermore, eqs. (3) and (4) can be used to calculate the base load (Q<sub>b</sub>) corresponding to the top load (Q<sub>t</sub>) and base displacement (w<sub>b</sub>) corresponding to the top displacement (w<sub>t</sub>), respectively. Subsequent to obtaining this set of Q<sub>b</sub> vs. w<sub>b</sub>, eqs. (3) and (4) can be inverted to the form shown in eqs. (5) and (6) to find the set of load and displacement at any selected depth z [i.e., Q<sub>(z)</sub> and w<sub>(z)</sub>, respectively] for the same set of top load (Q<sub>t</sub>) and top displacement (w<sub>t</sub>). Again, all L terms should be replaced with (L - z), as shown in eqs. (5) and (6).

$$w_{(z)} = \frac{Q_{(z)} \left[ 1 + \frac{4\eta \tanh[\mu(L-z)](L-z)}{\pi\lambda(1-v_s)\xi [\mu(L-z)] r_o} \right]}{G_{L(z)} r_o \left[ \frac{4\eta}{(1-v_s)\xi} + \frac{2\pi\rho_E \tanh[\mu(L-z)](L-z)}{\zeta [\mu(L-z)] r_o} \right]} \quad (2)$$

$$\frac{Q_b}{Q_t} = \frac{\left[ \frac{4\eta}{(1-v_s)\xi \cosh(\mu L)} \right]}{\left[ \frac{4\eta}{(1-v_s)\xi} + \frac{2\pi\rho_E \tanh(\mu L)L}{\zeta (\mu L) r_o} \right]} \quad (3)$$

$$\frac{w_b}{w_t} = \frac{1}{\cosh(\mu L)} \quad (4)$$

$$Q_{(z)} = \frac{Q_b \left[ \frac{4\eta}{(1-v_s)\xi} + \frac{2\pi\rho_E \tanh[\mu(L-z)](L-z)}{\zeta [\mu(L-z)] r_o} \right]}{\left[ \frac{4\eta}{(1-v_s)\xi \cosh[\mu(L-z)]} \right]} \quad (5)$$

$$w_{(z)} = w_b \cosh[\mu(L - z)] \quad (6)$$

where w<sub>(z)</sub> = pile total displacement at depth z below the top of pile's embedded length; Q<sub>(z)</sub> = portion of applied top load (Q<sub>t</sub>) transferred at depth z corresponding to w<sub>(z)</sub>; η = r<sub>b</sub>/r<sub>o</sub> = eta factor for underreamed piles (i.e., belled shafts); r<sub>o</sub> = d<sub>s</sub>/2 = pile shaft radius; r<sub>b</sub> = d<sub>b</sub>/2 = pile base radius; μ(L - z) = [2/(ζλ)]<sup>0.5</sup> · [(L - z)/r<sub>o</sub>] = measure of pile compressibility for the pile shaft segment between depth z and z = L; ζ = ln(r<sub>m</sub>/r<sub>o</sub>) = measure of average radius of influence in the surrounding soil mass affected by shearing stresses (i.e., the displacement field) around the pile; r<sub>m</sub> = (L - z) · {0.25 + ξ · [2.5 ρ<sub>E</sub>(1 - v<sub>s</sub>) - 0.25]} = average maximum influence radius along the embedded length of the pile [at this radius the shear stresses become negligible]; λ = E<sub>p</sub>/G<sub>L</sub> = pile-to-soil stiffness ratio; E<sub>p</sub> = pile modulus; G<sub>L</sub> = operative soil shear modulus at pile base (z = L); ξ = G<sub>L</sub>/G<sub>b</sub> = factor for end bearing piles resting on stiffer stratum (where G<sub>b</sub> > G<sub>L</sub>); G<sub>b</sub> = soil shear modulus below pile base (for z > L); ρ<sub>E</sub> = G<sub>M(z)}/G<sub>L</sub> = modulus variation factor (between selected depth z and at the pile base, where z = L); G<sub>M(z)</sub> = [G<sub>(z)</sub> + G<sub>L</sub>]/2 = operative soil shear modulus at mid of the pile length under consideration (between selected depth z and z = L); G<sub>(z)</sub> = operative soil shear modulus at depth z (at pile top, where z = 0, G<sub>(z)</sub> = G<sub>o</sub>); v<sub>s</sub> = Poisson's ratio of soil; w<sub>b</sub> = pile base displacement at depth z = L.</sub>

By using eqs. (5) and (6), sets of loads [Q<sub>(z)</sub>] and displacements [w<sub>(z)</sub>] can be calculated for selected depths (z) below the ground surface for a specific applied top load Q<sub>t</sub>. This exercise can be done for different applicable values of top loads. These sets can be further used to draw their respective shear stiffness reduction curves for selected depths from the back-analysis scheme presented in Niazi and Mayne (2015).

As a case illustration, this methodology was applied to a driven pile of length, L = 30.0 m, and diameter, d = 0.5 m. Sets of top loads (Q<sub>t</sub>) vs. top displacements (w<sub>t</sub>) were obtained using the modulus reduction algorithm for driven piles proposed in Niazi and Mayne (2015), which is reproduced in eq. (7) below:

$$\frac{G}{G_{\max}} = \frac{1}{1 + 3.04[\gamma_p(\%)]^{1.01}} \quad (7)$$

The soil modulus variation factor (ρ<sub>E</sub>) was selected over a wide range, with a value ρ<sub>E</sub> = 0.5 corresponding to a pure Gibson-type of soil stiffness profile (linear with depth), up to a value ρ<sub>E</sub> = 1.0, representing a constant soil stiffness profile with depth (i.e., homogeneous case). Simplified steps are presented in a flow chart shown in Figure 2, which enabled plotting of stiffness reduction curves corresponding to five depth levels: z = 0 (at the pile top), z = 0.25 L, z = 0.50 L (at pile mid depth), z = 0.75 L, and z = 1.00 L (at the pile tip) for different values of ρ<sub>E</sub>. These plots are shown in Figure 3. It may be noted that the thick curve with triangular markers representing soil modulus reduction near the ground surface, which is common in all 6 parts of Figure 3, was obtained from eq. (7). The remaining curves were drawn for different depths by following the steps shown in the flow chart. These curves clearly display the effect of progressive failure with depth and the influence of soil stiffness profile. Such curves can be drawn for any pile type and configuration, and for any soil profile. Subsequently, these curves can be used in a stacked pile model, which will be discussed in the following section.

### 3.2 Load Displacement Analysis of Stacked Pile Model in a Multi-layered Soil Medium

The basic form of elastic continuum solution, presented in eq. (1), works reasonably well for sites where the soil stiffness profile can be idealized as linear or general Gibson type. However, it is expected that certain sites may portray different trends of stiffness variation. For such situations, the pile may be modelled as a stack of shorter pile segments embedded through distinct multilayered soil media, with each layer having its own characteristic averaged stiffness value. As detailed previously, the tendency of stiffness reduction due to progressive failure can be quantified via slight adaptations in the basic solution to obtain stiffness reduction curves as function of depth. These trends can also be integrated into the solution of stacked pile model. In implementing such model, following vital assumptions are applicable:

- The number of layers is chosen on the basis of the measured stiffness profile of the soil, whereby each layer may be assigned its distinct mean modulus value. Thus, a constant stiffness profile is adopted for each layer.
- The component of the applied top load (Q<sub>t</sub>) reaching the bottom of the uppermost segments is taken as the base load for this segment (i.e., Q<sub>b1</sub>). This is calculated using eq. (3), and acts as the top load for the next segment below (i.e., Q<sub>t2</sub>). This applies to all subsequent layers (e.g., Q<sub>b1</sub> = Q<sub>t2</sub>, Q<sub>b2</sub> = Q<sub>t3</sub>, and so on).
- A similar approach is applied in calculating the ξ factor as the ratio of soil stiffness at the base of each segment. It implies that the mean stiffness value of the second soil layer is taken as the soil stiffness beneath the base of the top most segment, and the same applies to each of the subsequent segments and layers (i.e., G<sub>b1</sub> = G<sub>2</sub>, G<sub>b2</sub> = G<sub>3</sub>, and so on).
- The total displacement at the top of each segment is the cumulative displacement of all segments below it (e.g., for a three layered stacked pile model, the total displacement at the pile top = w<sub>t1</sub> + w<sub>t2</sub> + w<sub>t3</sub>, the total displacement at the top of second segment = w<sub>t2</sub> + w<sub>t3</sub>, and the displacement at the top of third and lower most segment = w<sub>t3</sub>).
- The pile length used in calculating the averaged maximum radius of influence of each segment is the pile distance between the top of that segment and the pile base (i.e., for a three layered stacked pile model, for the top most segment: use distance L<sub>1</sub> + L<sub>2</sub> + L<sub>3</sub>, for the middle segment: use distance L<sub>2</sub> + L<sub>3</sub>, and for the lower most segment: use distance L<sub>3</sub> only).
- The applicable values of operative soil stiffness for each layer and for each applicable load can be calculated from the scheme summarily presented in Figures 2 and 3.

**3.3 Application of the Proposed Solution**

For purposes of illustration, a four-layer stacked pile model is offered in Figure 4, where applicable equations of the solution are also presented, along with explanations of the relevant terms for each layer. This solution is slightly more involved compared to its basic form. However, it can be conveniently implemented in a spreadsheet, besides the fact that it is much less laborious than

alternative methods [e.g., Winkler springs support model by Mylonakis (2001), rigorous numerical solutions based on advanced

constitutive models of soil behavior proposed by Jardine et al. (1986), and the product of polynomial and series expansions of displacement shape functions in vertical and radial directions of infinite layer approach by Guo et al. (1987)].

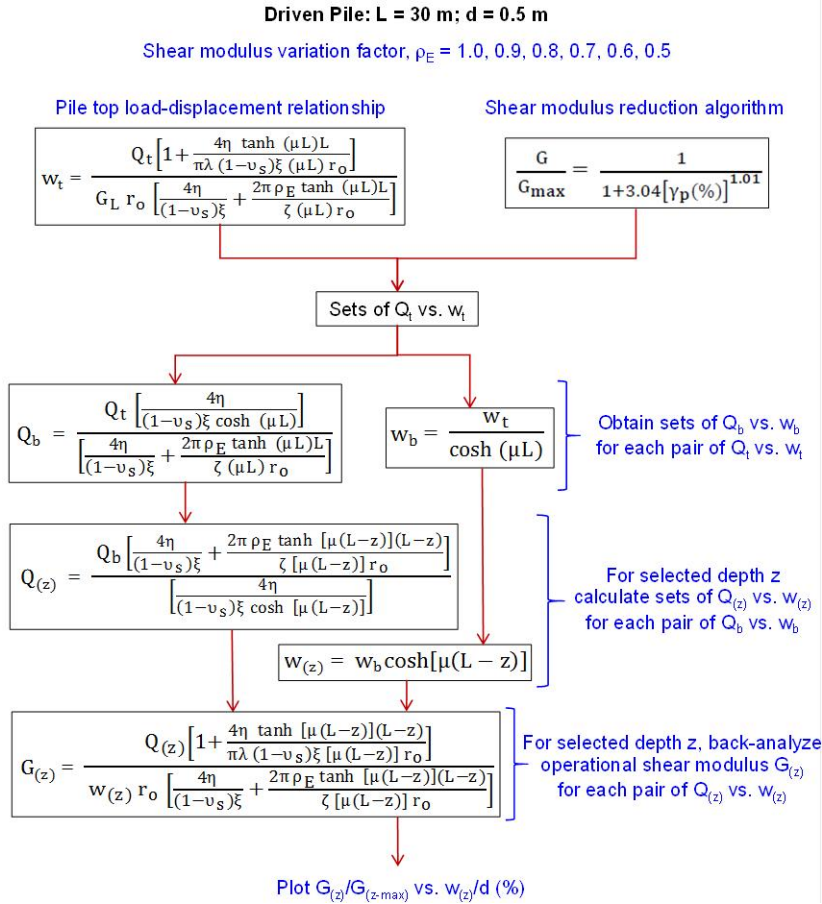


Figure 2 Flow chart showing example steps for plotting shear modulus reduction curves for selected depths using the solution for a compressible stacked pile model.

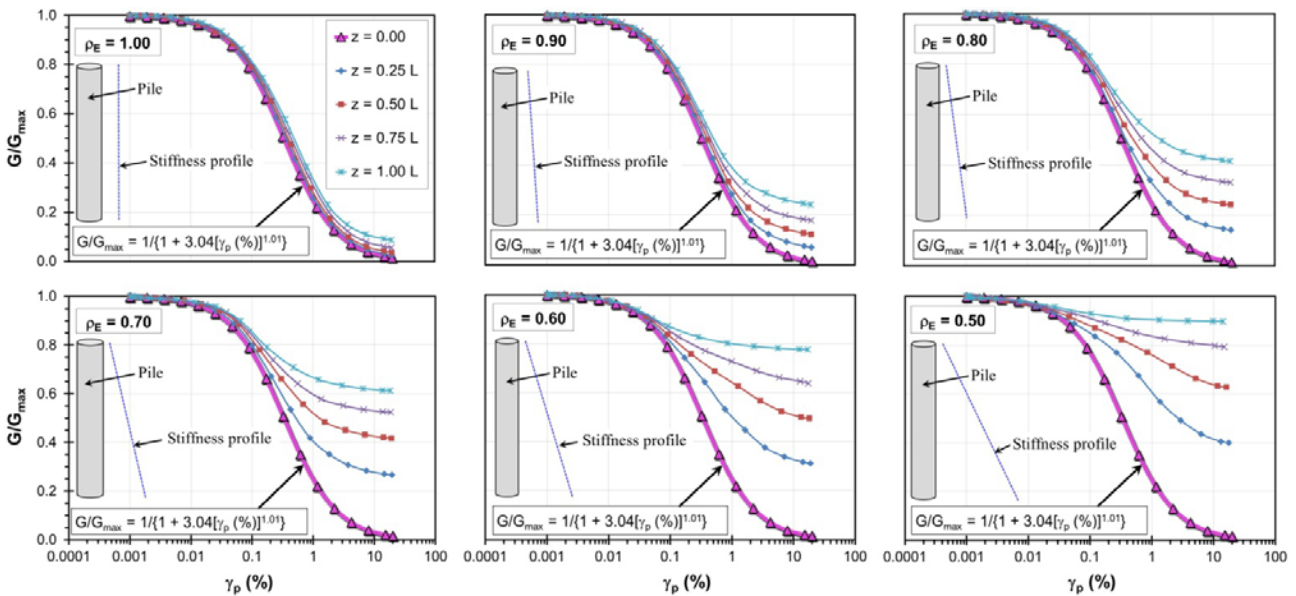
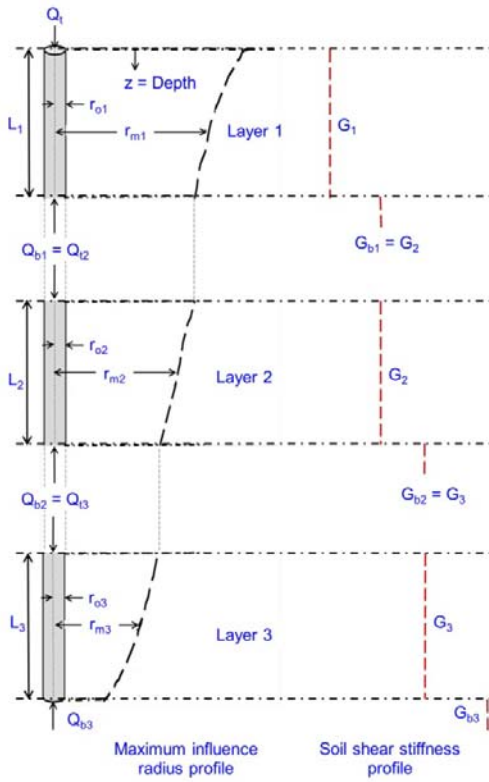


Figure 3 Illustration of shear modulus reduction curves as function of depth and soil stiffness variation profile.



**Solution for layer 1**

$$w_1 = \frac{Q_t \left[ 1 + \frac{4\eta_1 \tanh(\mu L_1) L_1}{\pi \lambda_1 (1 - \nu_{s1}) \xi_1 (\mu L_1) r_{o1}} \right]}{G_1 r_{o1} \left[ \frac{4\eta_1}{(1 - \nu_{s1}) \xi_1} + \frac{2\pi \rho_{E1} \tanh(\mu L_1) L_1}{\zeta_1 (\mu L_1) r_{o1}} \right]} + w_{12}$$

$$Q_{b1} = \frac{\left[ \frac{4\eta_1}{(1 - \nu_{s1}) \xi_1} \cosh(\mu L_1) \right]}{\left[ \frac{4\eta_1}{(1 - \nu_{s1}) \xi_1} + \frac{2\pi \rho_{E1} \tanh(\mu L_1) L_1}{\zeta_1 (\mu L_1) r_{o1}} \right]}$$

- $w_1$  = cumulative settlement at the pile top
- $\eta_1 = r_{o2}/r_{o1}$
- $\mu L_1 = [2/(\zeta_1 \lambda_1)]^{0.5} (L_1/r_{o1})$
- $\zeta_1 = \ln(r_{m1}/r_{o1})$
- $r_{m1} = (L_1 + L_2 + L_3) \{0.25 + \xi_1 [2.5 \rho_{E1} (1 - \nu_{s1}) - 0.25]\}$
- $\lambda_1 = E_p/G_1$
- $\xi_1 = G_{11}/G_{b1}$
- $G_{b1} = G_2$
- $\rho_{E1} = 1$
- $G_{M1} = G_{o1} = G_{L1} = G_1$
- $\nu_{s1}$  = Poisson's ratio of soil in layer 1
- $Q_{b1} = Q_{L2}$

**Solution for layer 2**

$$w_{12} = \frac{Q_{12} \left[ 1 + \frac{4\eta_2 \tanh(\mu L_2) L_2}{\pi \lambda_2 (1 - \nu_{s2}) \xi_2 (\mu L_2) r_{o2}} \right]}{G_2 r_{o2} \left[ \frac{4\eta_2}{(1 - \nu_{s2}) \xi_2} + \frac{2\pi \rho_{E2} \tanh(\mu L_2) L_2}{\zeta_2 (\mu L_2) r_{o2}} \right]} + w_{13}$$

$$Q_{b2} = \frac{\left[ \frac{4\eta_2}{(1 - \nu_{s2}) \xi_2} \cosh(\mu L_2) \right]}{\left[ \frac{4\eta_2}{(1 - \nu_{s2}) \xi_2} + \frac{2\pi \rho_{E2} \tanh(\mu L_2) L_2}{\zeta_2 (\mu L_2) r_{o2}} \right]}$$

- $w_{12}$  = cumulative settlement at the top of layer 2
- $\eta_2 = r_{o3}/r_{o2}$
- $\mu L_2 = [2/(\zeta_2 \lambda_2)]^{0.5} (L_2/r_{o2})$
- $\zeta_2 = \ln(r_{m2}/r_{o2})$
- $r_{m2} = (L_2 + L_3) \{0.25 + \xi_2 [2.5 \rho_{E2} (1 - \nu_{s2}) - 0.25]\}$
- $\lambda_2 = E_p/G_2$
- $\xi_2 = G_{22}/G_{b2}$
- $G_{b2} = G_3$
- $\rho_{E2} = 1$
- $G_{M2} = G_{o2} = G_{L2} = G_2$
- $\nu_{s2}$  = Poisson's ratio of soil in layer 2
- $Q_{b2} = Q_{L3}$

**Solution for layer 3**

$$w_{13} = \frac{Q_{13} \left[ 1 + \frac{4\eta_3 \tanh(\mu L_3) L_3}{\pi \lambda_3 (1 - \nu_{s3}) \xi_3 (\mu L_3) r_{o3}} \right]}{G_3 r_{o3} \left[ \frac{4\eta_3}{(1 - \nu_{s3}) \xi_3} + \frac{2\pi \rho_{E3} \tanh(\mu L_3) L_3}{\zeta_3 (\mu L_3) r_{o3}} \right]}$$

$$Q_{b3} = \frac{\left[ \frac{4\eta_3}{(1 - \nu_{s3}) \xi_3} \cosh(\mu L_3) \right]}{\left[ \frac{4\eta_3}{(1 - \nu_{s3}) \xi_3} + \frac{2\pi \rho_{E3} \tanh(\mu L_3) L_3}{\zeta_3 (\mu L_3) r_{o3}} \right]}$$

$$w_{b3} = \frac{w_{13}}{\cosh(\mu L_3)}$$

- $w_{13}$  = settlement at the top of layer 3
- $\eta_3 = r_p/r_{o3}$
- $\mu L_3 = [2/(\zeta_3 \lambda_3)]^{0.5} (L_3/r_{o3})$
- $\zeta_3 = \ln(r_{m3}/r_{o3})$
- $r_{m3} = L_3 \{0.25 + \xi_3 [2.5 \rho_{E3} (1 - \nu_{s3}) - 0.25]\}$
- $\lambda_3 = E_p/G_3$
- $\xi_3 = G_{33}/G_{b3}$
- $G_{b3}$  = shear stiffness beneath pile base
- $\rho_{E3} = 1$
- $G_{M3} = G_{o3} = G_{L3} = G_3$
- $\nu_{s3}$  = Poisson's ratio of soil in layer 3
- $w_{b3}$  = displacement at the pile base

Figure 4 Analytical elastic continuum solution for compressible stacked pile model in four-layer soil medium.

**3.4 Solution for Rigid Piles**

A simplified version of the analytical elastic solution for a stacked pile model in the case of rigid driven piles in four-layer soil media is summarized in Figures 5 and 6. This solution can also be applied to other categories of rigid piles (bored, augered, and jacked) by using their applicable stiffness reduction algorithms [such as those presented in Mayne and Niazi (2015)]. The applicable expressions of the closed-form solution for rigid piles are also reproduced below:

$$w_t = \frac{Q_t}{G_L r_o \left[ \frac{4\eta}{(1 - \nu_s)\xi} + \frac{2\pi \rho_E L}{\zeta r_o} \right]} \tag{8}$$

$$Q_b = \frac{Q_t}{\left[ 1 + \frac{\pi \rho_E (1 - \nu_s) \xi L}{2 \zeta \eta r_o} \right]} \tag{9}$$

$$w_b = w_t \tag{10}$$

$$Q_{(z)} = Q_b \left[ 1 + \frac{\pi \rho_E (1 - \nu_s) \xi (L - z)}{2 \zeta \eta r_o} \right] \tag{11}$$

$$G_{(z)} = \frac{Q_{(z)}}{w_{(z)} r_o \left[ \frac{4\eta}{(1 - \nu_s)\xi} + \frac{2\pi \rho_E (L - z)}{\zeta r_o} \right]} \tag{12}$$

**3.5 Case of Homogeneous Soils**

It may be noticed from the two models presented in Figures 4 and 6 that the stiffness profiles in the layered media represent a general Gibson type soil since the stiffness appears to increase linearly with depth. These models were preferred in view of a common observation noted from the database used in the companion paper, where at a predominant majority of the sites the stiffness increases linearly with depth. These models can, however, be simplified and

utilized for a homogeneous soil as well, where a straight vertical line may be drawn through all the discretized layers representing the average stiffness value for the entire pile length. The models and the equations shown in Figures 4 and 6 will still be applicable except for a fact that all the parameters derived from the small-strain (fundamental) soil stiffness ( $G_{max}$ ) profile (i.e.,  $\lambda_i$ ,  $\xi_i$ ,  $\rho_{Ei}$  etc., where subscript  $i$  represents the  $i^{th}$  layer) will have the same values for all the layers.

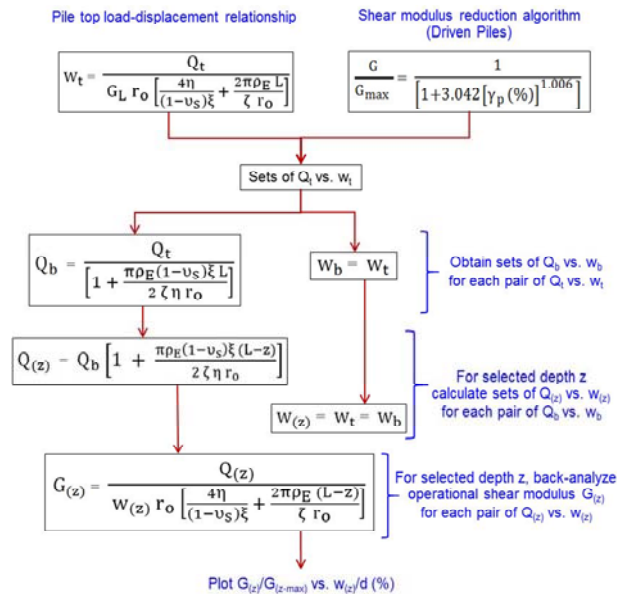


Figure 5 Flow chart showing solution steps for plotting shear modulus reduction curves for selected depths for rigid stacked pile model.

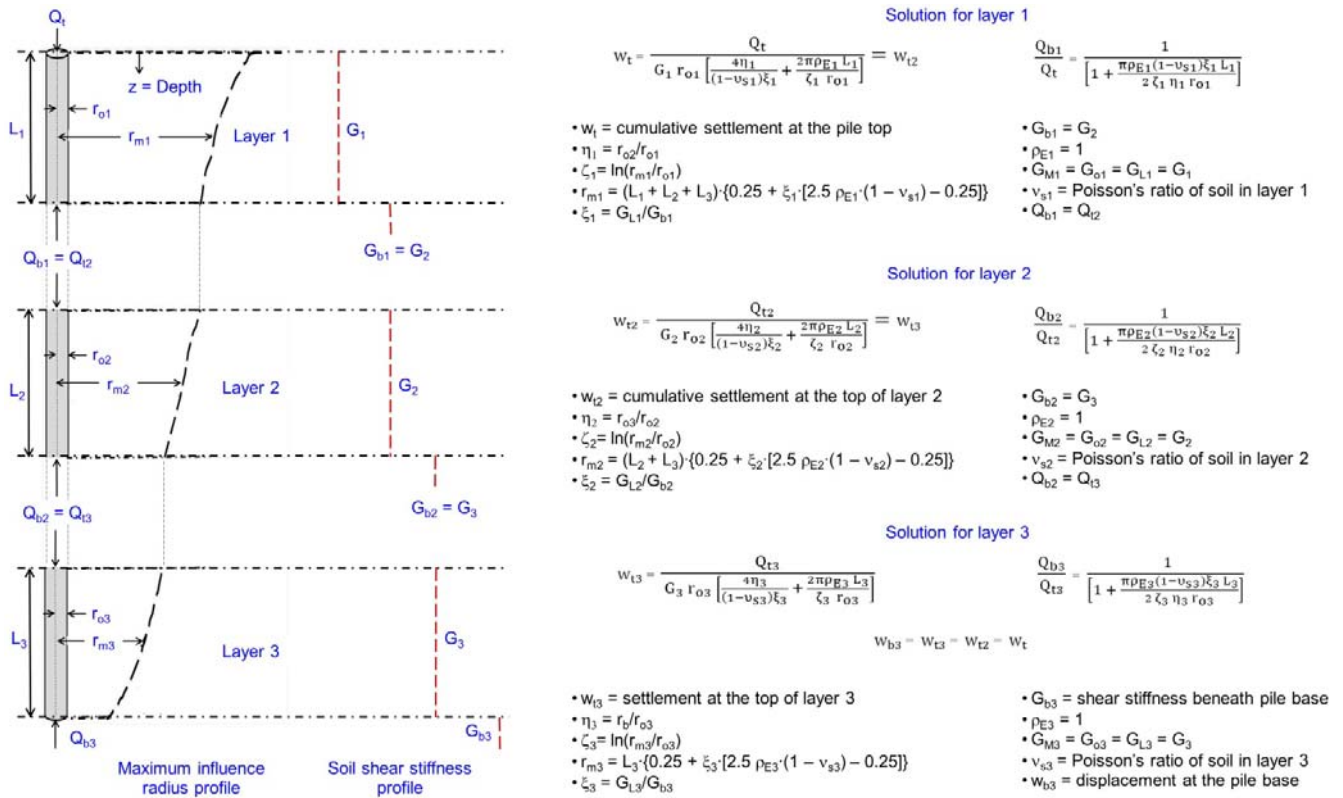


Figure 6 Analytical elastic continuum solution for rigid stacked pile model in four-layer soil medium.

However, treating a homogeneous soil as a layered media provides a step improvement over the earlier simplified model of the companion paper because the influence radii ( $r_m$ ) of the discretized layers have been developed to account for progressive failure (or variable "operative stiffness") with depth, i.e., only applicable pile lengths below the top levels of different layers are used in the respective  $r_m$  calculations. As presented in Figure 3, the overall difference in the operative stiffness at varying depths for the case of homogeneous soil ( $\rho_E = 1$ , i.e., the top left graph of that figure) may be minor compared to the other cases presented in the same figure. Nevertheless, the combined effects of the: (1) well-defined operative stiffness for different depths, and (2) improved description of the influence radii for those layers are likely to result in overall enhanced evaluations of the pile load-settlement response.

### 3.6 Application of the Proposed Model to a Case Study of Load Test on Bored Pile at Grimsby Research Site, UK

The Grimsby research site is located near Waltham, Grimsby, UK, 900 m north of the nearest watercourse and 7.5 km southwest of the nearest coastline. Brown et al. (2006) report the ground conditions at the site as matrix-dominant glacial till underlain by cretaceous chalk bedrock; till being cohesive, over consolidated stiff to firm, grayish to dark brown, predominantly silty clay with cobbles, boulders and pebbles. Index properties include liquid limit: 20 – 36%, plastic limit: 12 – 18%, moisture content: 14 – 24%, and clay fraction: 20 – 38%. Prior to the load test on a 12.08-m long and 0.6-m diameter bored pile, extensive site and laboratory investigations were conducted. Of particular interest for this study is the  $V_s$  profile obtained from a 20-m deep SCPTu sounding (see Figure 7). The pile testing program was designed to compare the results from rapid and static load tests: rapid load test (RLT) being performed first, followed by constant rate of penetration (CRP) test at 0.01 mm/s and maintained load test (MLT) (Brown et al. 2006), and Brown (2004). For this study, the results measured only from the CRP test are considered, as these are more standardized and representative of the field conditions compared to the MLT.

Before treating the stratum at the site as a layered soil medium, a first order approximation of stiffness profile was done by forcing a best-fit line through the calculated  $G_{max}$  data, resulting in general Gibson type soil trend (see Figure 7). This approximation was utilized in employing the methodology detailed in section 3.1 to derive stiffness reduction curves as a function of depth for different layers shown in Figure 8.

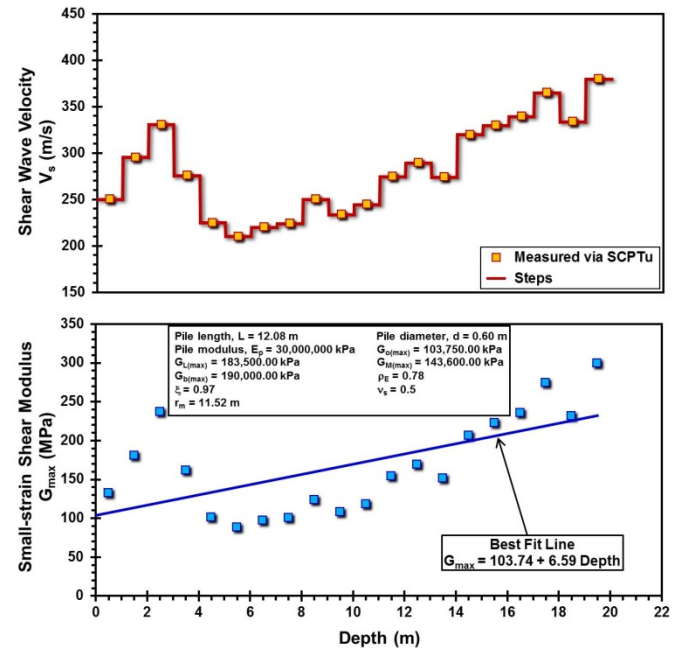


Figure 7 Shear wave velocity from SCPTu and small-strain shear modulus profiles at Grimsby Research Site, UK (Brown et al. 2006).

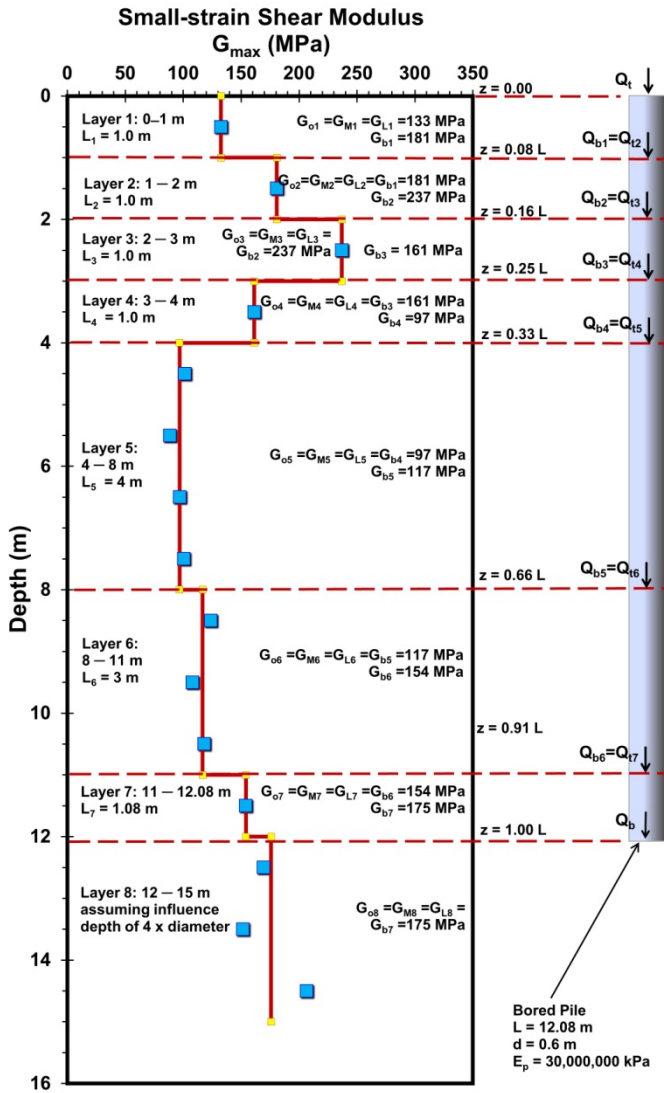


Figure 8 Discretization of the stratum into eight-layered soil medium based on the stiffness profile.

The stratum corresponding to the embedded pile length was broken into eight layers based on the  $G_{max}$  data. The layers along with their average  $G_{max}$  values are shown in Figure 8. The generalized expression developed in eq. (15) of the companion paper was used to plot the basic stiffness reduction curve from the selected top settlements ( $w_i$ ) and their corresponding top loads ( $Q_i$ ). This curve is shown by the thick dashed line in Figure 9(a). Here, the adjustment factors  $\alpha_1 = 1.91$ , and  $\beta_1 = 0.97$  were adopted for bored pile, while  $\alpha_2$  and  $\beta_2$  were calculated as 1.07 and 0.99, respectively, for average plasticity index (PI) of 14% along the embedded pile length. A Poisson's ratio of 0.5 was selected to represent undrained conditions. The sets of  $Q_{(z)}$  and  $w_{(z)}$  calculated for the remaining seven layers per the procedure explained in section 3.1 were then used along with the same eq. (15) of the companion paper to plot their respective stiffness reduction curves as shown in Figure 9(a). For convenience in calculations, a depth adjustment factor  $\delta$  was introduced to represent curves corresponding to different layers [see Figure 9(b)].

The stiffness reduction trends thus obtained were integrated into the proposed stacked pile model for this bored pile. This model represents the original pile considered as seven smaller pile segments stacked over the other as shown in Figure 8. Here, the base loads of the upper segments were taken as the top loads for the lower segments. According to the procedure outlined in section 3.2, complete sets of loads vs. displacements ( $Q-w$ ) were obtained for each segment in their corresponding layers. Their respective stiffness reduction curves from Figure 9 were used in calculations for these  $Q-w$  sets. Complete sets of the analytical elastic solutions for different layers are presented in Figure 10, where all the parameters used in their respective calculations are listed.

The results are presented in Figure 11, where part (a) shows the outcome of the evaluations from the elastic continuum solution using simpler approximation of stiffness profile from Figure 7, while part (b) shows the results from implementing the stacked pile model summarized above. Clearly, the later model presents a response which compares better with the measurements taken during the load test, besides the fact that it also provides more detailed picture of the loads transfer, and settlements mechanism for the same pile. In the first site, this solution may appear more convoluted; however, a spreadsheet application is much simpler to implement.

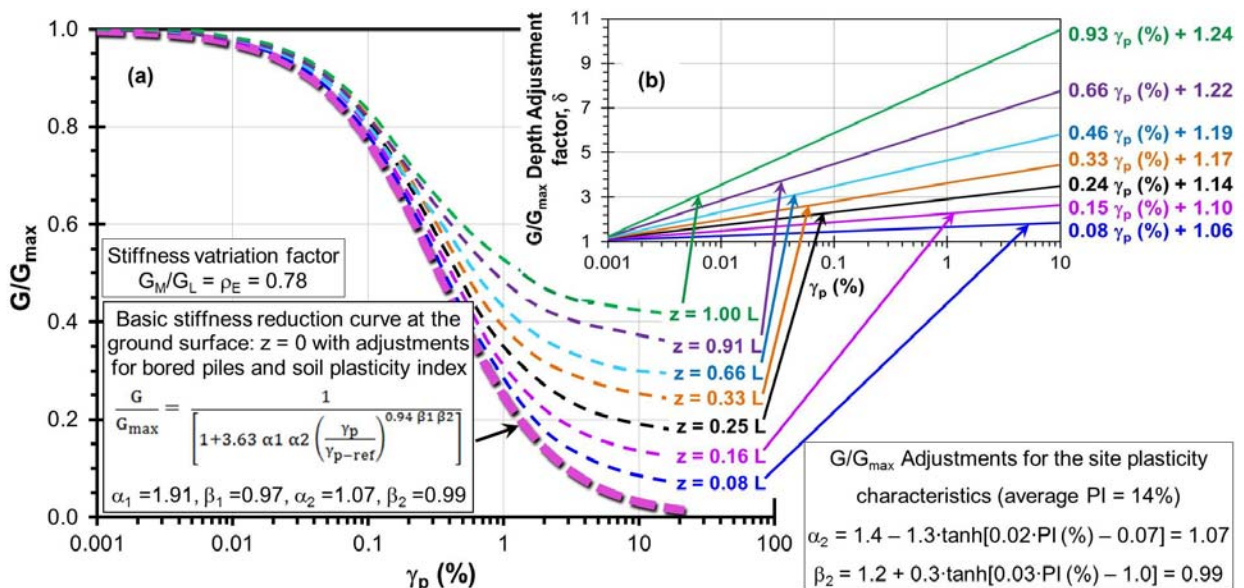


Figure 9 Stiffness reduction curves for 12.08-m long, 0.6-m diameter bored pile load tested at Grimsby Research Site, UK

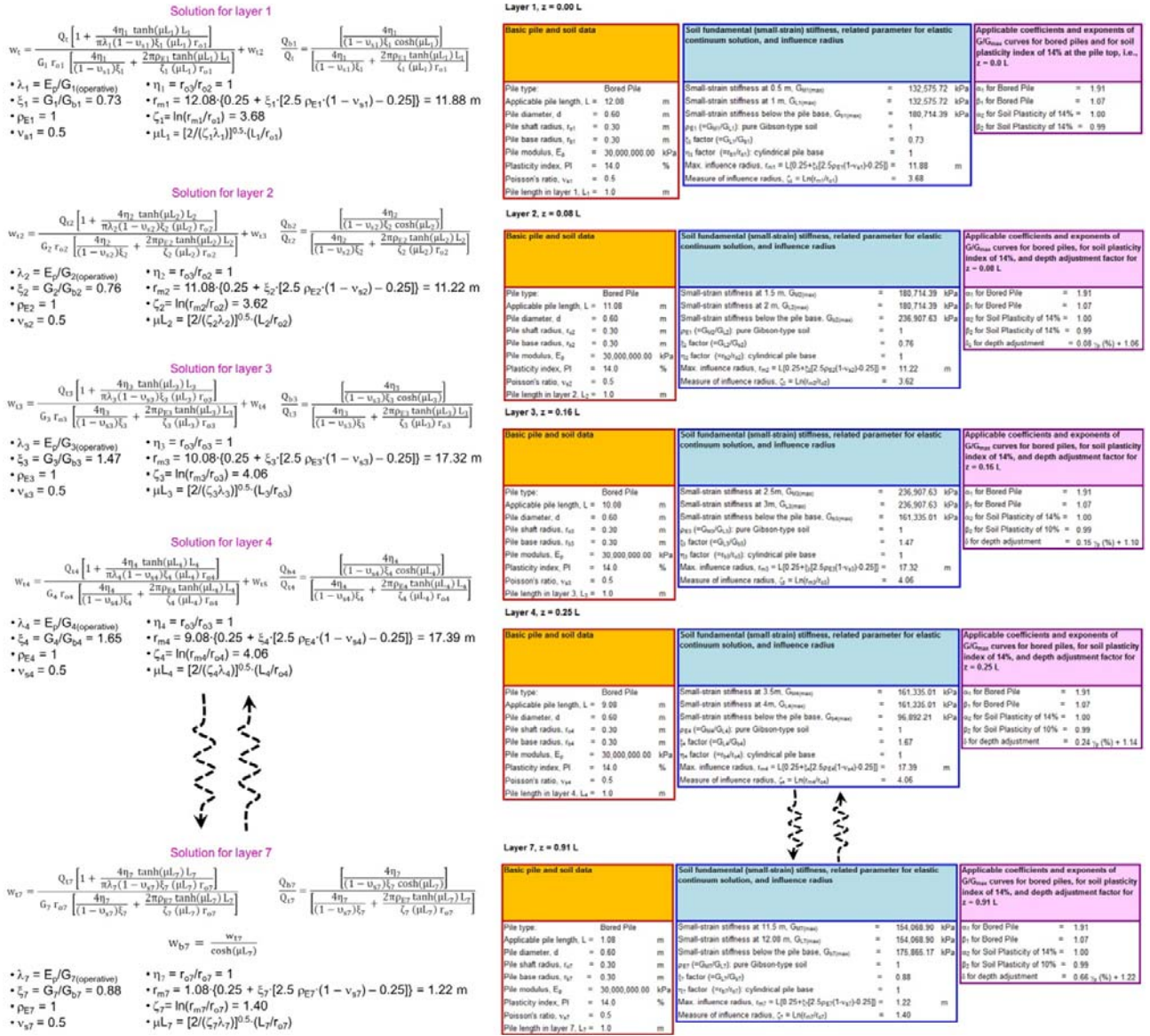


Figure 10 Analytical elastic continuum solution for compressible stacked pile model in eight-layered soil media at Grimsby Research Site, UK.

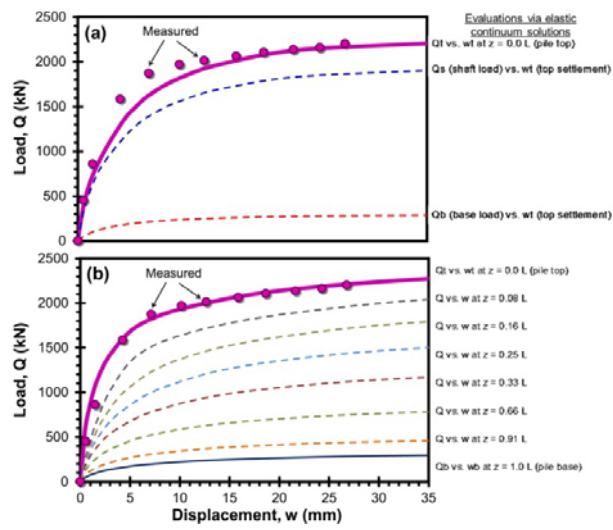


Figure 11 Results of load-displacement evaluations: (a) approximate analytical elastic continuum solution; (b) stacked pile model.

#### 4. CONCLUSIONS

A stacked pile model for load-displacement analysis is presented in which certain adaptations are proposed in the elastic continuum solution. These adaptations enable plotting of separate modulus reduction curves ( $G/G_{max}$  vs.  $w/d$ ) as function of depth for each layer, and treating pile as a stack of smaller pile segments embedded in a multi-layered soil medium, where the mean operative stiffness of each layer is adopted for the purpose of analysis. The solution can be used to address the question of progressive failure with depth in a multi-layer soil medium that exhibits nonlinear soil stiffness response. It is a step towards further refinement in the use and extended application of Randolph elastic continuum pile solutions from the improvements presented in the companion paper by Niazi and Mayne (2015).

#### 5. ACKNOWLEDGMENTS

The authors would like to acknowledge the generosity and support provided by ConeTec Investigations of Richmond, BC, Canada towards these research interests and findings.

## 6. REFERENCES

- Brown, M. J. (2004). "The rapid load testing of piles in fine grained soils." Ph.D. Thesis, University of Sheffield, UK: 151 – 198.
- Brown, M. J., Hyde, A. F. L. and Anderson, W. F. (2006). Analysis of a rapid load test on an instrumented bored pile in clay. *Géotechnique*, 56(9): 627 – 638.
- Cooke, R.W. 1974. "The settlement of friction pile foundations." *Proceedings of the Conference on Tall Buildings*, Kuala Lumpur, Malaysia.
- Cooke, R. W., Price, G. and Tarr, K. (1979). "Jacked piles in London Clay: a study of load transfer and settlement under working conditions." *Géotechnique*, 29(2): 113 – 147.
- Frank, R. (1975). "Etude théorique du comportement des pieux sous charge verticale." *Rapporte de Recherché No. 46*, Laboratoire Central des Ponts et Chaussées, Paris, France.
- Guo, D. J., Tham, L. G. and Cheung, Y. K. (1987). "Infinite layer for the analysis of a single pile." *Computers and Geotechnics*, Vol. 3: 229 – 249.
- Jardine, R. J., Potts, D. M., Fourie, A. B. and Burland, J. B. (1986). "Studies of the influence of non-linear stress-strain characteristics in soil-structure interaction." *Géotechnique*, 36(3): 377 – 396.
- Mylonakis, G. (2001). "Winkler modulus for axially-loaded piles." *Géotechnique*, 51(5): 455 – 461.
- Niazi, F. S. and Mayne, P. W. (2015). "Operational soil stiffness from back-analysis of pile load tests within elastic continuum framework." *SEAGS-AGSSEA Journal* (companion paper in this issue).
- Randolph, M. F. (2007). *Manual PIGLET: Analysis and design of pile groups*. Version 5.1, Centre for Offshore Foundation Systems, School of Civil and Resource Engineering, The University of Western Australia, Crawley, Western Australia: 35 p.
- Randolph, M. F. and Wroth, C. P. (1978). "Analysis of deformation of vertically-loaded piles." *ASCE Journal of the Geotechnical Engineering Division*, 104(GT12): 1465 – 1488.
- Randolph, M. F. and Wroth, C. P. (1979). "A simple approach to pile design and the evaluation of pile tests." *Behavior of Deep Foundations*, STP 670, ASTM, West Conshohocken, PA: 484 – 499.